

A Longitudinal Diffeomorphic Atlas-Based Tissue Labeling Framework for Fetal Brains using Geodesic Regression

Roxane Licandro^{1,2}

licandro@caa.tuwien.ac.at

¹ Institute of Computer Aided Automation, Computer Vision Lab, Vienna University of Technology,
<http://www.caa.tuwien.ac.at/cvl>

² Department of Radiology and Image-guided Therapy, Computational Imaging Research Lab,
Medical University of Vienna,
<http://www.cir.meduniwien.ac.at>

Georg Langs²

Gregor Kasprian²

Robert Sablatnig¹

Daniela Prayer²

Ernst Schwartz²

Abstract. *The human brain undergoes structural changes in size and in morphology between the second and the third trimester of pregnancy, corresponding to accelerated growth and the progress of cortical folding. To make fetal brains comparable, spatio-temporal atlases are used as a standard space for studying brain development, fetal pathology locations, fetal abnormalities or anatomy. The aim of this work is to provide a continuous model of brain development and to use it as base for an automatic tissue labeling framework. This paper provides a novel longitudinal fetal brain atlas construction concept for geodesic image regression using three different age-ranges which are parametrized according to the developmental stage of the fetus. The dataset used for evaluation contains 45 T2-weighted Magnetic Resonance (MR) volumes between Gestation Week (GW) 18.0 and GW 30 day 2. The automatic tissue labeling framework estimates cortical segmentations with a Dice Coefficient (DC) of up to 0.85 and ventricle segmentations with a DC of up to 0.60.*

1. Introduction

The aim of brain mapping experiments is to create maps (models), based on studies, to understand structural and functional brain organization. To this end, neuroimaging methods as well as knowledge of neuroanatomy and physiology are combined. Due to the fundamental changes occurring in the human fe-

tal brain during pregnancy, a single map is not sufficient to model brain development [19]. Changes in size, according to accelerated growth, changes in morphology, due to the progress of cortical folding and deceleration of the proliferation of ventricular progenitor cells [16] occur and are illustrated in Figure 1a. Thus, a collection of brain maps is needed to describe these alterations as a function of time. For studying the brain organisation during its development, abnormalities, and locations of pathologies, brain maps are used as a reference model [18]. Newly acquired brain images are labelled to identify structures and possible abnormal changes or to find indicators for diseases. This labeling can be performed manually by annotating the images, which needs an expert, time and consequently leads to increased costs compared to an automatic labeling procedure [3]. In this case, labels for non annotated images are estimated automatically by software using a brain model for the mapping. Such an automated labeling procedure on the one hand and a reference model on the other form an atlas. To cover the time-dependent development of the fetal brain, time-varying reference models are considered for building spatio-temporal atlases.

1.1. State-of-the-Art

State-of-the-art approaches [8, 10, 13, 17, 21] for computing a spatio-temporal atlas combine registration methods and interpolation techniques to obtain

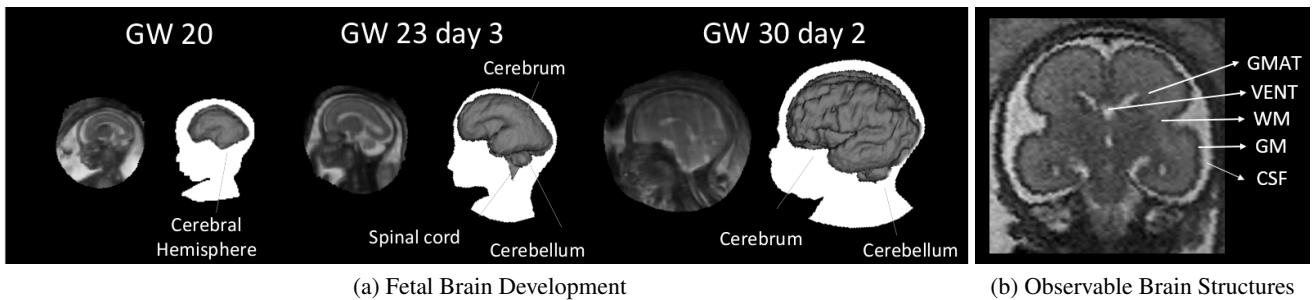


Figure 1: Left: MR imaging and schematic illustration of the fetal brain development at GW 20, 23 day 3 and 30 day 2. Right: Illustration of identifiable brain structures in a T2 weighted fast MR image acquired with a 1.5 Tesla scanner (Grey Matter (GM), White Matter (WM), the VENTricles (VENT) and the Germinal MATrix (GMAT) [21]). Also extraventricular Cerebro Spinal Fluid (CSF), Deep Grey Matter (DGM) and Non-Brain structures (NB), like skull or amniotic fluid are identifiable. MR images courtesy of Medical University of Vienna (MUW).

continuity in time. The use of an "all-to-one" approach (a single subject as reference) introduces substantial bias. The brain structures of fetuses cannot be described by one image, since it does not reflect occurring changes over time [10, 17]. Exclusive pairwise affine registration for image alignment results in blurred regions in the templates obtained by intensity averaging. Affine registration is not capable of compensating local inter-subject variability [17]. This leads to worse registration results between atlas-based segmentations and individual objects compared to non-rigid approaches, which show a higher level of detail [17]. An advantage of pairwise approaches lies in the registration of wider age-ranges between 15 to 18 Gestation Weeks (GW), compared to groupwise approaches, which are able to cover only small age ranges between 5 to 8 GW. A benefit of groupwise registration approaches is the template-free estimation of the initial reference space. The template is estimated and updated during the registration procedure [10]. The main limitations of groupwise registration lie in the lower level of anatomic definition [17]. Examples for pairwise approaches can be found in [10, 17] and for groupwise approaches in [8, 13, 21].

1.2. Challenges

Imaging of a fetus in utero is challenging, due to its constantly changing position, which causes image unsharpness and artefacts [5]. Thus, a main issue in fetal imaging lies in shortening the image acquisition time to 20 seconds and to use motion correction techniques [4]. The Magnetic Resonance (MR)

imaging technique is used as an alternative to ultrasonography for prenatal diagnosis and is able to image a fetus in a non-invasive way. Distinguishable brain structures using this technique are illustrated in Figure 1b. A problem of MR imaging is the lack of comparability and constancy of gray-values. Thus, for the comparison of brains of adult patients, an atlas as a standard space is required, which avoids the gray-value discrepancies. The brains are mapped to a standardized coordinate system according to marked anatomical locations. However, the fetal brain is a developing structure. In comparison to building an atlas of an adult brain, the fast change of a fetal brain in shape and size has to be taken into account [10]. Also, fetal brains at a certain GW show differences in orientation shape and size. Possible reasons are the inaccuracy in determination of the gestational age, inter-patient variability or pathological growth processes [15]. The motivation for building a fetal atlas is the possibility to compare fetal brains for studying brain development, fetal pathology locations, fetal abnormalities or anatomy.

1.3. Contribution

We create a tissue labeling framework for cortical and ventricle structures in the fetal brain from GW 18 to GW 30. An automatic segmentation procedure including a longitudinal fetal brain atlas and a labeling procedure are considered. In our work we demonstrate that image regression is capable to build a spatio-temporal atlas of the fetal brain and is able to model a mean trajectory encoding the brain development in a single diffeomorphic defor-

mation, instead of calculating discrete age-dependent templates combined with interpolation. As found in literature [7, 9, 11], image regression for time-series data have been evaluated only using adult- and child-brain datasets, which record changes of brain structure over time. In the proposed work the local inter-subject variability is considered to be modelled continuously in time and non-rigidly in space by geodesic regression [1, 2]. The computed atlas is used as a prior of the Graph Cut (GC) approach for multi label segmentation proposed by Yuan et al. [20].

The paper is organized as follows. In Section 2 an overview of the methodology used and the concept of the tissue labeling framework proposed is presented. The results and the corresponding discussion are given in Section 3. This work concludes with a summary of the contributions in Section 4.

2. Methodology

The framework proposed is illustrated in Figure 2. The input represents a gray value image I_{new} at time point t_{new} , which is preprocessed in a first step, by performing motion correction, rigid alignment, image masking and image cropping. Subsequently, the longitudinal diffeomorphic fetal brain atlas is used to estimate a time point t_{new} corresponding diffeomorphic transformation for computing a time-dependent intensity image I_A and a time-dependent segmentation for ventricular and cortical tissue S_A^{tissue} in atlas space. In a pairwise registration procedure, a transformation T from the preprocessed input (*Aligned* I_{new}) to the atlas-based intensity image I_A is estimated. The inverse of the computed transformation T^{-1} is used to transform the atlas based segmentations S_A^{tissue} to the subject's space ($S_A^{tissue} \circ T^{-1} = S_{GC}^{tissue}$). As next step the transformed segmentations S_{GC}^{tissue} and I_{new} are used as input parameters for the multi label GC segmentation refinement. The output of the framework are segmentations for ventricular and cortical brain tissues S_{new}^{tissue} of the input image I_{new} .

2.1. Image Acquisition and Preprocessing

The time series MR image dataset used consists of 45 healthy fetal brains with an age range between 18 and 30 GW. The MR image acquisition is performed using an 1.5 Philips Gyroscan superconducting unit scanner performing a single-shot, fast spin-echo T2-weighted MR sequence: In-plane resolu-

tion = 0.78 - 0.9 pixels per mm, Slice thickness = 3 - 4.4mm, Acquisition matrix = 256×256, Field of view = 200 - 230mm, Specific Absorption Rate (SAR) = < 100% /4.0W/kg, Image acquisition time = ≤ 20s, TE (Echo Time) = 100 - 140ms, TR (Repetition Time) = 9000 - 19000ms. The dataset of MR images used for atlas learning are preprocessed using the pipeline illustrated in Figure 2. First the images are motion corrected using the toolkit for fetal brain MR images published by Rousseau et al. [14]. Subsequently, the manual annotation of the cortex, left and right eye, ventricle and occipital foramen magnum is performed by an expert. After this step, the data is rigidly aligned, the surrounding mother tissue is excluded in a masking step and the volumes are cropped to reduce computational costs in the longitudinal registration procedure using a bounding box of size 90 × 140 × 140 voxels.

2.2. Spatio Temporal Atlas Learning

The algorithm used for Diffeomorphic Anatomical RegistraTion using Exponential Lie algebra (DARTEL) of Ashburner et al. [1, 2] for geodesic regression is integrated in the Statistical ParaMetric (SPM) tool box - release SPM8 ¹. This approach is used to encode the brain development in a single diffeomorphic deformation by optimising the energy term E expressed in Equation 1 [2].

$$E = \frac{1}{2} \|Lv_0\|^2 + \frac{1}{2} \sum_{n=1}^N \left(\int_{x \in \Omega} \|I_{t_0} - I_{t_n}(\varphi_{t_n})\|^2 dx \right) \quad (1)$$

The term φ_{t_n} denotes the forward deformation from source I_{t_0} to target I_{t_n} at time point t_n , where $n = 1, \dots, N$ and L represents a model of the "inertia" of the system, i.e. a linear operator which operates on a time-dependent velocity that mediates the deformation over unit time [2]. It is introduced to derive an initial momentum m_0 through an initial velocity v_0 . The velocity field $v(x)$ learned at position x is parametrised using a linear combination of i basis functions. Such basis functions consist of a vector of coefficients c_i and a i^{th} first degree B-spline basis function $\rho_i(x)$ (cf. Equation 2) [1].

$$v(x) = \sum_i c_i \rho_i(x) \quad (2)$$

The aim of the DARTEL implementation is to estimate an optimized parametrisation of c . The energy

¹<http://www.fil.ion.ucl.ac.uk/spm/>; [accessed 07 December 2015]

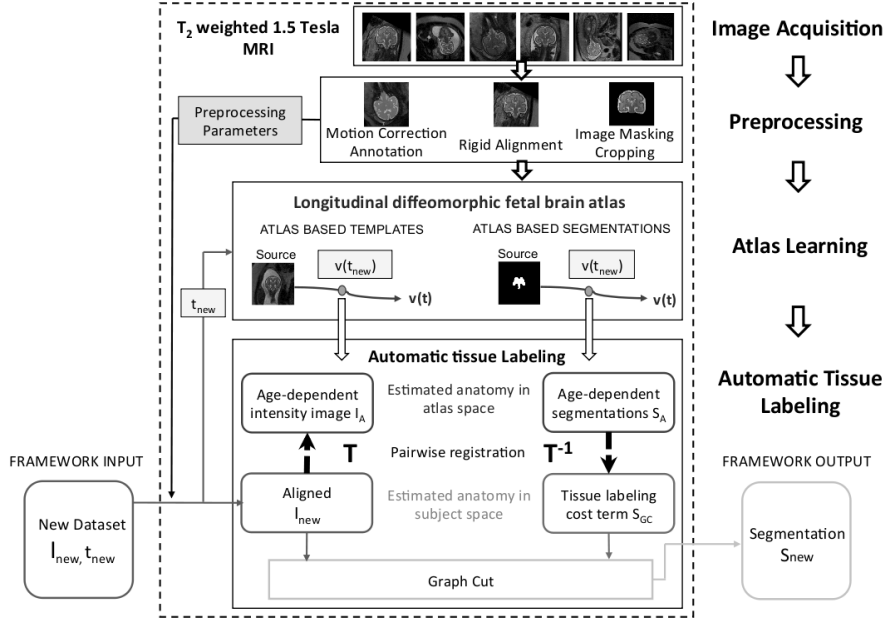


Figure 2: Fetal brain tissue labeling framework. MR images courtesy of MUW.

cost term E in Equation 1 is reformulated in terms of finding the coefficients of c for a given dataset D with maximum probability (cf. Equation 3). A maximization of the probability leads to the minimization of its negative logarithm and thus, is used to interpret registration of data D as a minimization procedure of the objective function ($-\log p(c, D)$) expressed in Equation 3, consisting of a prior term ($-\log p(c)$) and a likelihood term ($-\log p(D|c)$) [1].

$$-\log p(c, D) = -\log p(c) - \log p(D|c) \quad (3)$$

The prior term denotes the prior probability $p(c)$. Ashburner et al. [1] use a concentration matrix (inverse of a covariance matrix) K to encode spatial variability. The parameters $[\lambda_1, \lambda_2, \lambda_0, \lambda, \mu]$, which have to be predefined to compute K , influence the behaviour of the deformation (bending energy, stretching, shearing) as well as the divergence and amount of volumetric expansion or contraction [1]. The term λ_0 encodes the penalisation of absolute displacements, λ_1 penalises the difference between two neighboured vectors by observing the first derivatives (linear term) of the displacements, λ_2 penalises the difference between the first derivatives of two neighboured vectors by observing the second derivatives of the displacements and λ denotes the variability of the spatial locations (divergence of each point in the flow field) with a constant value. Increasing λ leads to increasing smoothing of the flow vector field and preserves volumes during the transformation. The

term μ encodes the variance according to symmetric components, rotations and the penalisation of scaling and shearing. The likelihood term encodes the probability of c given the data D [1] and corresponds to the mean-squared difference between a warped template deformed by the calculated transformation and the target image.

2.2.1 Optimisation Procedure

A Full Multi Grid (FMG) approach is used to solve the equation (cf. Equation 4) which is needed to update the vector field during a Gauß-Newton optimising procedure, where H^{iter} denotes the Hessian, g^{iter} the gradient and K the concentration matrix. Details regarding the computation of v_0^{iter+1} are explained in [1, 2].

$$v_0^{iter+1} = v_0^{iter} - \epsilon(K + H^{iter})^{-1}(Kv_0^{iter} + g^{iter}) \quad (4)$$

For this task images are observed in different scales. For every resolution level multigrid methods recursively estimate the field, starting at the coarsest scale and computing the residual to solve the update equations on the current grid. Subsequently, the solution is prolonged to the next finer grid [1].

2.3. Automatic Tissue Labeling using Graph Cuts

For tissue labeling, we use a continuous max flow formulation of a multi label GC [20]. Three input parameters are necessary for performing tissue segmentation. A data term (gray value volume I_{new}

at age t_{new}), a cost (unary) term, and a penalty (binary) term. For computing a unary term, atlas based segmentations for cortex and ventricle tissue $S_{tissue} = \{S_{cortex}, S_{ventricle}\}$ at age t are estimated and smoothed with a Gaussian filter G . The parameter δ is defined to weight the smoothed result with a constant factor. The unary term is illustrated in Equation 5, where \star denotes the convolution operator.

$$C = \delta * (S_{tissue} \star G) \quad (5)$$

Three different binary terms are evaluated:

Penalty term 1 (P_1) is a weighted norm of the gradient of the data term D (cf. Equation 6), where δ denotes the same weighting term as used in Equation 5 and a, b are constant weighting parameters.

$$P_1 = \delta * \frac{b}{1 + (a * \|\nabla D\|)} \quad (6)$$

Penalty term 2 (P_2) denotes an intensity based term and is calculated separately for cortex and ventricle segmentation (cf. Equation 7). Tissue type specific gray values are modelled as Gaussian distributions $N \sim (\mu_{tissue}, \sigma_{tissue})$, which parameters μ_{tissue} and σ_{tissue} are estimated using the a-priori atlas segmentation. These parameters are used to calculate the probability of every pixel belonging to cortex or ventricle. Subsequently, the gradient of the resulting probability map P and its norm are computed and weighted by the parameters δ, a, b as shown in Equation 6.

$$P_2 = \delta * \frac{b}{1 + (a * \|\nabla P(\mu_{tissue}, \sigma_{tissue})\|)} \quad (7)$$

Penalty term 3 (P_3) represents an exponential formulation and is expressed in Equation 8. The parameter u is a constant and v a linear weighting parameter. The term w weights the norm of the image's D gradient non-linearly in the exponential term.

$$P_3 = u + v * \exp\left(-\frac{\|\nabla D\|}{w}\right) \quad (8)$$

3. Results

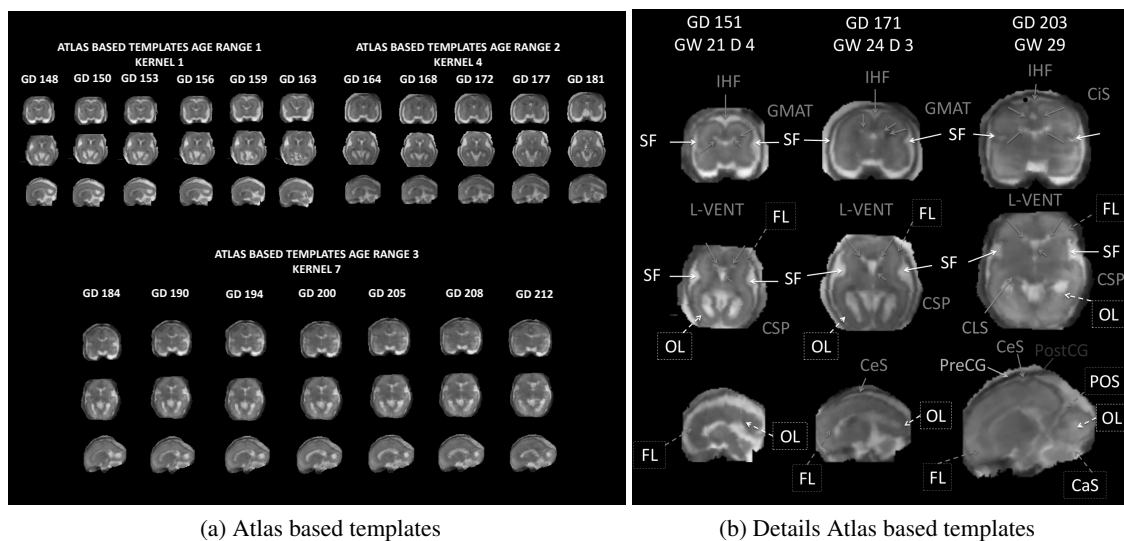
Evaluation of the proposed framework is performed using leave-one-out cross validation. In this paper a novel longitudinal registration procedure is formulated by dividing the data set into three age ranges, based on the developmental stage of the fetus. Age range 1 reaches from 20 GW day 6 (146 GD) to 23 GW day 3 (164 GD), age range 2 from 23 GW

day 3 (164 GD) to 26 GW day 2 (184 GD) and age range 3 from 26 GW day 2 (184 GD) to 30 GW day 2 (212 GD). The first part of the evaluation documents the atlas learning results for each age range. Subsequently, the atlases computed are used to evaluate the tissue labeling procedure as a second part of the evaluation. Estimated atlas templates at the testing time-point are pairwise registered to the test MR volume to obtain a transformation T . The inverse T^{-1} is used to transform the atlas based segmentation to the test-subject's space. As last step the segmentation of the test volume using the transformed atlas is computed. To evaluate our approach, we report the overlap between automatic- and manual segmentations of the fetal cortex and ventricles. In the leave-one-out cross validation, we compare the Dice Coefficient (DC) [6] between the groundtruth annotation and different automatic segmentations based on (1) the atlas, (2) the transformed atlas, and (3) the GC segmentation optimization.

Furthermore, we report the volume of cortex and ventricles, and the area of the cortical surface of the atlas based segmentations.

3.1. Results Spatio-Temporal Atlas Learning

The deformation behaviour of image regression using 21 different regularisation kernels $K[\lambda_1, \lambda_2, \lambda_0, \lambda, \mu]$ (cf. Section 2.2) is evaluated for every age range. Beside the DC also the behaviour of the regularisation of the volume expansion and changes of the area of cortical surface have to be taken into account, when choosing a suitable kernel. Atlas-based cortical and ventricle segmentations are studied. According to the evaluation results, kernel 1 ($K_1 [0.01, 0.01, 9e^{-6}, 1e^{-5}, 1e^{-5}]$) is chosen as suitable regularisation for age range 1, kernel 4 ($K_4 [0.01, 9e^{-6}, 9e^{-6}, 0.01, 1e^{-5}]$) for age range 2 and kernel 7 ($K_7 [0.01, 0.01, 9e^{-6}, 0.01, 1e^{-5}]$) for age range 3. Figure 3a shows examples of the atlas templates learned and Figure 3b illustrates the anatomical details of these at age GW 21 day 4 (GD 151), GW 24 day 3 (GD 171) and GW 29 (GD 203). In both figures the growth of the brain structures is observable. The brain model at age range 1 is characterised by a smoother cortex surface in comparison to a brain at a higher age range. It also visualises the increase of the cortical folding grade. According to Pugash et al. [12], the ventricles achieve their thickest size in early gestation and regress in the third trimester, which is not visible. The regularisa-



(a) Atlas based templates

(b) Details Atlas based templates

Figure 3: Left: Atlas based templates of age range 1, 2 and 3 between GW 21 day 1 (GD 148) and GW 30 day 2 (GD 212). Right: Anatomical details of atlas based templates at age GW 21 day 4 (GD 151), GW 24 day 3 (GD 171) and GW 29 (GD 203). Coronal (first row), axial (second row) and sagittal (third row) slices are illustrated. Denoted structures: Sylvian Fissure (SF), InterHemispheric Fissure (IHF), Germinal MATrix (GMAT), Lateral-VENTricle (L-VENT), Cingulate Sulcus (CiS), ColLateral Sulcus (CLS), Cavum of Septum Pellucidum (CSP), Occipital Lobe (OL), Frontal Lobe (FL), Central Sulcus (CeS), PreCentral Gyrus (PreCG), PostCentral Gyrus (PostCG), ParietoOccipital Sulcus (POS) and Calcarine Sulcus (CaS).

tion term for geodesic regression is not able to model location specific volume expansion and shrinkage at the same time. This leads to worse modelling results for ventricles, compared to cortical structure, since a kernel is chosen which models expansion. Additionally, the subject specific variability of age-dependent ventricle size in the dataset and the complex form of ventricles complicate the determination of a suitable kernel and consequently the registration procedure. Observable structures at every age range are Sylvian Fissures (SF), Lateral VENTricle (L-VENT), Inter-Hemispheric Fissure (IHF), Cavum of Septum Pellucidum (CSP), Occipital Lobe (OL) and Frontal Lobe (FL). The SF show in the coronal and axial slices a smooth bending at age range 1 and develop to a deep fold at the lateral side of the brain at age range 3. Also the IHF shows a deeper folding at age range 3 with Cingulate Sulcus (CiS) as additional forming compared to age range 1. The Germinal MATrix (GMAT) is existent until age range 2 and disappears later in the third trimester of pregnancy. The Central Sulcus (CeS) formation starts at age range 2 and gets more apparent at age range 3 as well as the developing of the PreCentral Gyrus (PreCG) and PostCentral Gyrus (PostCG). The ColLateral Sulcus (CLS) is visible at age range 3 as well as the Calcarine Sulcus

(CaS) and PreOccipital Sulcus (POS).

3.2. Results Automatic Tissue Labeling

For pairwise registration kernel A ($K_A [5e^{-3}, 5e^{-3}, 3e^{-5}, 1e^{-5}, 9e^{-6}]$) is used for regularisation. The DC distributions of segmentations of the cortex for age range 1, 2 and 3 are illustrated in Figure 4 on the top and for ventricle segmentations on the bottom. The DC distribution of atlas based and transformed atlas-based segmentations using pairwise registration are illustrated and the three dotted lines visualise the DCs of GC based segmentations computed using penalty terms 1, 2 and 3. For age range 1 the highest DC improvement from 0.727 to 0.771 at GD 158 is achieved by pairwise registration and GC refinement compared to atlas based segmentations. In contrast to this no improvement is reached at GD 151, but shows the highest DC of about 0.851. At GDs older than 154 the GC refining using penalty 1 and penalty 2 achieve a higher DC increase of about 0.02 compared to using penalty 3. At age range 2 no improvement of transformed atlas based segmentations is observed after pairwise registration, which leads to a decrease of the DC. It is observed that the labeling result of the pairwise registration

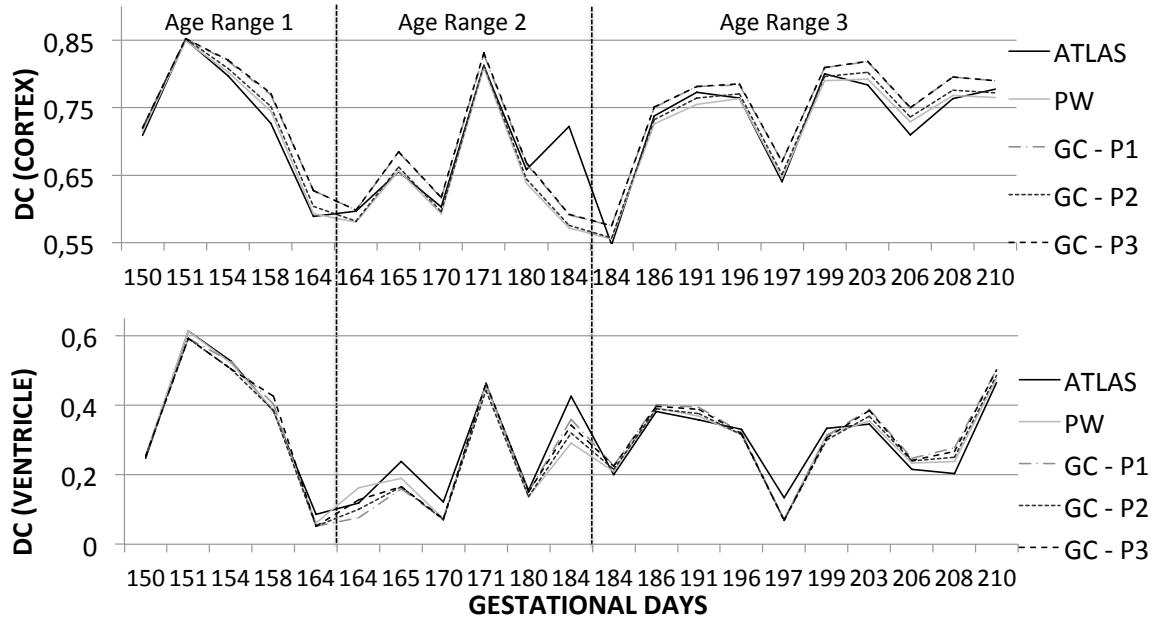


Figure 4: DCs of automatically estimated labels of the cortex and ventricle at age range 1, 2 and 3.

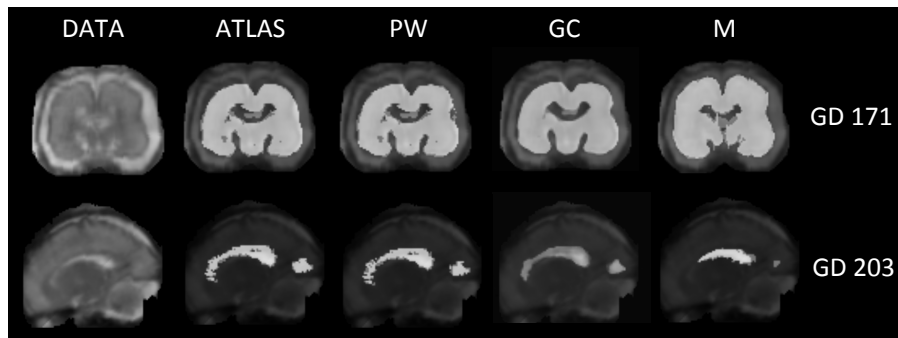


Figure 5: Top: Coronal view - segmentations of the cortex at GD 171 (GW 24 day 3), bottom: sagittal view - segmentations of the ventricle at GD 203 (GW 29). Segmentations are illustrated estimated by the atlas (ATLAS), after the pairwise registration procedure (PW), estimated by the GC approach (GC) and manual annotations (M).

has an influence on the GC labeling since it acts as initialization of this procedure, best visible at GD 184. The GC refinement is able to compensate the results of the pairwise registration between GD 164 and 184 and shows an increase of the DC between atlas and graph-cut based segmentations in average of about 0.02. At age range 3 an increase of DC at every age range is achievable using GC refinement. The highest improvement between atlas-based segmentations and GC based segmentations is reached at GD 206 with a DC increase from 0.71 to 0.795. The highest DC at age range 3 of about 0.819 is achieved at GD 203 and the lowest of about 0.575 at GD 184. It is observable that pairwise registration

is not capable to compensate differences in volume size or absolute displacements. If an estimated segmentation has a bigger volume than the structure to be segmented or is displaced, then the borders of neighbored tissue prevents the GC approach from cutting through regions of a high gradient, since this would lead to increasing costs in the energy minimisation procedure. Consequently, the GC is not capable to refine the segmentation. In Figure 5 an example for a misaligned segmentation and its deformation through the labeling procedure is illustrated. The displacement is observable at the IHF in the first column and the superior part of the anterior horn of the ventricle in the second column. Test

data and corresponding estimated segmentations, transformed segmentations to subject's space and GC based segmentations of the cortex at GD 171 (top) and of ventricular tissue at GD 203 (bottom) are shown. The GC segmentations are computed using the penalty term 3, since it shows the best improvement between atlas-based and GC based segmentations.

4. Conclusion

In this paper an automatic fetal brain tissue labeling framework using geodesic image regression was presented and was identified to be suitable as registration approach to longitudinally model the changes of the brain during the 18th and 30th GW. The advantage is the provision of a time-dependent transformation from a source to a target brain, instead of combining a template building technique and interpolation technique to obtain continuity in time. A novel longitudinal registration scheme was proposed, using separate age ranges for flexible regularisation of the deformation behaviour due to the age range dependent changes. The atlas learned was evaluated using a leave-one-out cross validation approach for every age range and 21 different regularisation kernels were analysed according to their behaviour regarding volume expansion, modelling of cortical surface and Dice similarity to manual annotations. The fetal brain atlas proposed is not capable of modelling the thinning of ventricles from age range 1 to age range 3. Since the proposed method uses one regularisation kernel per age range, geodesic regression is not able to regularise location specific volume expansion and shrinkage at the same time. To overcome this issue, the usage of tissue specific regularisation and consequently the computation of separate ventricle atlases are a possible solution. In contrast to this, the increase of the cortical folding grade and of the volume over time are integrated in the proposed spatio-temporal model. The quality of transformed atlas based segmentations to subject's space using pairwise registration leads to the conclusion that the kernel for pairwise registration has to be defined differently according to the age range and also tissue type, for being able to improve the graph cut initialisation term. Additionally, it is shown that the quality of graph cut labeling is dependent on the initialisation cost term (atlas segmentation) and the penalty term. A false or displaced atlas segmentation hinders as cost term the refinement of the graph cut based

labeling. Finally the proposed framework is able to estimate cortex segmentations with a DC up to 0.85 and ventricle segmentations up to 0.60. We show that image regression is capable to model the variability of fetal brains in time and is qualified to be used for building a spatio-temporal atlas as basis for fetal brain tissue segmentation. The evaluation of the cortical labeling results for age range 1, 2 and 3 show that a single kernel for pairwise registration for every age range is not suitable. Thus, a main focus of future work will lie in the improvement of the labeling procedure, by evaluating age range and tissue dependent regularisation, to improve the quality of graph cut based segmentation. Additionally, a combination of global rigid and local deformable pairwise registration could be analysed for transforming atlas based segmentations to the subject's space as extension to this work.

Acknowledgements

This work was co-funded by ZIT - Life Sciences 2014, grant number 1207843, Project Flowcluster, and by OeNB (15929).

References

- [1] J. Ashburner. A fast diffeomorphic image registration algorithm. *NeuroImage*, 38(1):95–113, Oct. 2007. 3, 4
- [2] J. Ashburner and K. Friston. Diffeomorphic registration using geodesic shooting and Gauss-Newton optimisation. *NeuroImage*, 55(3):954–967, Apr. 2011. 3, 4
- [3] M. Becker and N. Magnenat-Thalmann. Deformable models in medical image segmentation. In N. Magnenat-Thalmann, O. Ratib, and H. Choi, editors, *3D Multiscale Physiological Human*, pages 81–106. Springer London, Jan. 2014. 1
- [4] L. Breyssem, H. Bosmans, S. Dymarkowski, D. V. Schoubroeck, I. Witters, J. Deprest, P. Demaerel, D. Vanbeckevoort, C. Vanhole, P. Casaer, and M. Smet. The value of fast MR imaging as an adjunct to ultrasound in prenatal diagnosis. *European Radiology*, 13(7):1538–1548, July 2003. 2
- [5] M. Clemence. How to shorten MRI sequences. In D. Prayer, editor, *Fetal MRI*, Medical Radiology, pages 19–32. Springer Berlin Heidelberg, 2011. 2

- [6] L. Dice. Measures of the amount of ecologic association between species. *Ecology*, 26(3):297–302, July 1945. 5
- [7] S. Durrleman, X. Pennec, A. Trouvé, J. Braga, G. Gerig, and N. Ayache. Toward a comprehensive framework for the spatiotemporal statistical analysis of longitudinal shape data. *International Journal of Computer Vision*, 103(1):22–59, May 2013. 3
- [8] P. Habas, K. Kim, J. Corbett-Detig, F. Rousseau, O. Glenn, A. Barkovich, and C. Studholme. A spatiotemporal atlas of MR intensity, tissue probability and shape of the fetal brain with application to segmentation. *NeuroImage*, 53(2):460–470, Nov. 2010. 1, 2
- [9] Y. Hong, Y. Shi, M. Styner, M. Sanchez, and M. Niethammer. Simple geodesic regression for image time-series. In B. Dawant, G. Christensen, J. Fitzpatrick, and D. Rueckert, editors, *Biomedical Image Registration*, number 7359 in Lecture Notes in Computer Science, pages 11–20. Springer Berlin Heidelberg, Jan. 2012. 3
- [10] M. Kuklisova-Murgasova, P. Aljabar, L. Srinivasan, S. Counsell, V. Doria, A. Serag, I. Gousias, J. Boardman, M. Rutherford, A. Edwards, J. Hajnal, and D. Rueckert. A dynamic 4D probabilistic atlas of the developing brain. *NeuroImage*, 54(4):2750–2763, Feb. 2011. 1, 2
- [11] M. Niethammer, Y. Huang, and F. Vialard. Geodesic regression for image time-series. *International Conference MICCAI 2011*, 14(Pt 2):655–662, 2011. 3
- [12] D. Pugash, U. Nemeč, P. Brugger, and D. Prayer. Fetal MRI of Normal Brain Development. In D. Prayer, editor, *Fetal MRI*, Medical Radiology, pages 147–175. Springer Berlin Heidelberg, Jan. 2011. 5
- [13] L. Risser, F. Vialard, A. Serag, P. Ajabar, and D. Rueckert. Construction of diffeomorphic spatio-temporal atlases using Krcher means and LDDMM: Application to early cortical development. In *Workshop on Image Analysis of Human Brain Development (IAHBD)*, in *International Conference MICCAI 2011*, Sept. 2011. 1, 2
- [14] F. Rousseau, E. Oubel, J. Pontabry, M. Schweitzer, C. Studholme, M. Koob, and J. Dietemann. BTK: An Open-Source Toolkit for Fetal Brain MR Image Processing. *Computer methods and programs in biomedicine*, 109(1):65–73, Jan. 2013. 3
- [15] T. Saul, R. Lewiss, and M. Rivera. Accuracy of emergency physician performed bedside ultrasound in determining gestational age in first trimester pregnancy. *Critical Ultrasound Journal*, 4(1):1–5, Dec. 2012. 2
- [16] J. Scott, P. Habas, K. Kim, V. Rajagopalan, K. Hamzelou, J. Corbett-Detig, A. Barkovich, O. Glenn, and C. Studholme. Growth trajectories of the human fetal brain tissues estimated from 3D reconstructed in utero MRI. *International Journal of Developmental Neuroscience*, 29(5):529–536, Aug. 2011. 1
- [17] A. Serag, P. Aljabar, G. Ball, S. Counsell, J. Boardman, M. Rutherford, A. Edwards, J. Hajnal, and D. Rueckert. Construction of a consistent high-definition spatio-temporal atlas of the developing brain using adaptive kernel regression. *NeuroImage*, 59(3):2255–2265, Feb. 2012. 1, 2
- [18] C. Studholme. Mapping fetal brain development in utero using magnetic resonance imaging: the big bang of brain mapping. *Annual review of biomedical engineering*, 13:345–368, Aug. 2011. 1
- [19] A. Toga and P. Thompson. 1 - an introduction to maps and atlases of the brain. In A.W. Toga and J.C. Mazziotta, editors, *Brain Mapping: The Systems*, pages 3–32. Academic Press, San Diego, 2000. 1
- [20] J. Yuan, E. Bae, X. Tai, and Y. Boykov. A continuous max-flow approach to potts model. In K. Daniilidis, P. Maragos, and N. Paragios, editors, *Computer Vision ECCV 2010*, number 6316 in Lecture Notes in Computer Science, pages 379–392. Springer Berlin Heidelberg, Jan. 2010. 3, 4
- [21] J. Zhan, I. Dinov, J. Li, Z. Zhang, S. Hobel, Y. Shi, X. Lin, A. Zamanyan, L. Feng, G. Teng, F. Fang, Y. Tang, F. Zang, A. Toga, and S. Liu. Spatialtemporal atlas of human fetal brain development during the early second trimester. *NeuroImage*, 82:115–126, Nov. 2013. 1, 2